MATHEMATICAL BIOSCIENCES
AND ENGINEERING
Volume **9**, Number **1**, January **2012**

doi:10.3934/mbe.2012.9.175

pp. **175–198**

A QUASI-LUMPED MODEL FOR THE PERIPHERAL DISTORTION OF THE ARTERIAL PULSE

Panagiotes A. Voltairas and Antonios Charalambopoulos
and Dimitrios I. Fotiadis

Department of Materials Science, University of Ioannina
GR 451 10, Ioannina, Greece

Lambros K. Michalis

Department of Cardiology, Medical School, University of Ioannina
GR 451 10, Ioannnina, Greece

(Communicated by Mette Olufsen)

Abstract. As blood circulates through the arterial tree, the flow and pressure pulse distort. Principal factors to this distortion are reflections form arterial bifurcations and the viscous character of the flow of the blood. Both of them are expounded in the literature and included in our analysis. The nonlinearities of inertial effects are usually taken into account in numerical simulations, based on Navier-Stokes like equations. Nevertheless, there isn't any qualitative, analytical formula, which examines the role of blood's inertia on the distortion of the pulse. We derive such an analytical nonlinear formula. It emanates from a generalized Bernoulli's equation for an an-harmonic, linear, viscoelastic, Maxwell fluid flow in a linear, viscoelastic, Kelvin-Voigt, thin, cylindrical vessel. We report that close to the heart, convection effects related to the change in the magnitude of the velocity of blood dominate the alteration of the shape of the pressure pulse, while at remote sites of the vascular tree, convection of vorticity, related to the change in the direction of the velocity of blood with respect to a mean axial flow, prevails. A quantitative comparison between the an-harmonic theory and related pressure measurements is also performed.

1. **Introduction.** Variations in the form of the arterial pressure and flow pulse are often used as clinical indicators of cardiovascular diseases [41]. Therefore, it is important to gain an understanding of the underlying mechanisms that constitute the arterial pulse in normal physiology. Each beat of the heart creates a pressure wave which travels along the arterial network, changing shape as it moves away from the heart. The amplitude of the flow wave, or pulse, decreases monotonically with the distance from the heart. The same applies to the pressure pulse but only at remote locations of the arterial network. This is due to viscous dissipation, accompanied by the viscoelasticity of the vessel wall. Nevertheless, initially, the systolic peak of the pressure pulse increases, as it travels away from the heart. In the arterial periphery, about half period after the systolic peak, a secondary peak, the diastolic peak, appears. In addition, irregularities of the proximal waveform

2000 *Mathematics Subject Classification.* 92C35, 74D05, 76A10, 76F10, 74J99.

Key words and phrases. Arterial pulse modeling, fluid-structure interaction, viscoelasticity, wave propagation, Klein-Gordon equation, vascular disease.

D. I. Fotiadis and L. K. Michalis are also with the Biomedical Research Institute-FORTH, University of Ioannina.

Nomenclature

$\mathbf{A}$, $\mathbf{A}_h$	vector potentials
$\mathcal{A}$, $\mathcal{A}_h$	radial parts of $\mathbf{A}$ and $\mathbf{A}_h$
b_i, $i = 1, 2, 3$	constants in P_s
$c_q^{(a)}$, $c_q^{(b)}$	dimensionless constants
C_i, D_i, $i = 0, 1, 2, v$	"viscoelastic" constants of the arterial wall
$\mathbf{D}_b$	rate of deformation tensor
De_b	Blood Deborah number
De_a	Artery Deborah number
$\mathbf{e}_i$, $i = r, \theta, z$	unit vectors
f_b	normal stress on the arterial wall due to blood
$\mathbf{f}_h$	impulsive body force due to heart
F_b, F_d	dimensionless normal stresses on the arterial wall due to blood
$G(\tau_a, \eta_a)$	Green's function
h	arterial wall thickness
k	Mach's to convection number product
$\mathbf{L}_b$	velocity gradient
L	characteristic length
L_v	viscoelastic length constant
$\mathcal{L}$	linear viscoelasticity operator
$\mathbf{n}$	normal unit vector on $\mathrm{S}(t)$
p, p_s, p_{ref}	dimensionless pressures
$P(t, z)$	pressure
$P_s(t)$	solitary pressure pulse
P_0	characteristic pressure constant
P_{ref}	reference pressure
q	order of $\psi_q^{(b)}$, $\psi_q^{(a)}$
Q	volumetric flow rate in artery
r	radial coordinate
$r_a = R$	radius of deformed artery
R_0	radius of un-deformed artery
Re	Reynolds number
$S(t)$	deformed arterial wall surface
t	time
$\mathbf{T}_b$	viscoelastic stress tensor
t_a, t_b	viscoelastic time constants
t_0	characteristic time constant
$\mathbf{u}$	blood velocity vector
$\langle u \rangle$	average flow pulse
u_r	radial component of $\mathbf{u}$
u_z	axial component of $\mathbf{u}$
u_0	characteristic velocity constant
u_a, u_b	pulse velocities
u_c	mean axial blood velocity constant
u_{ref}	reference blood velocity per vessel
u_A	amplitude of $\langle u \rangle$
U_a, U_b	inverse of Mach's numbers
U_c	Convection number
z	axial coordinate

Greek letters

α, α_h, α_z	dimensionless radial functions, with α_z corresponding to u_z
β, β_v	dimensionless length to radius ratios
γ	dimensionless constant
δ	dimensionless densities ratio
ε_b, ε_a	dimensionless constants
E	Young modulus of elasticity
ζ	dimensionless constant related to axial velocity profile modes
η_b, η_a	dimensionless axial coordinates
Θ	dimensionless part of the radial wall displacement
$\mathbf{I}$	identity tensor
I_s	dimensionless temporal integral part of ξ_s
κ	dimensionless constant related to ζ
$\mathbf{K}$	harmonic vector potential
λ_e, λ_v	elastic and viscous Lame constants
μ_e, μ_v	elastic and viscous Lame constants
μ_b	shear viscosity of blood
M_a, M_b	Mach's numbers
$\boldsymbol{\xi}$	displacement vector of the arterial wall
$\xi_s(t)$	temporal axial displacement function
ξ_m	mean radial displacement constant
ρ_a, ρ_b	densities
$\sigma(h)$, σ_0	Poisson's ratios
τ_b, τ_a	dimensionless time coordinates
$\tau_s^{(b)}$	wall shear stress
$\Phi^{(b)}$, $\Phi^{(a)}$	dimensionless spatiotemporal functions
χ	dimensionless constant
$\Psi^{(b)}$, $\Psi^{(a)}$, $\psi_q^{(b)}$, $\psi_q^{(a)}$	dimensionless spatiotemporal functions
$\boldsymbol{\omega}$	vorticity vector
$\Omega(t)$	blood flow region

(like the dicrotic notch: a notch in the pressure pulse that marks the closure of the aortic valve) are smoothed out peripherally. A long-standing problem is the interpretation of these flow and pressure pulse distortions in terms of physiological factors (cardiac output, blood's viscosity, vessel wall elasticity, mean flow velocity, etc.) and geometrical characteristics of the arterial network (distance from the heart, vessel diameter, degree of bifurcation of the arterial network, etc.). A range of models have been proposed for this purpose, like: Fourier [30] and wave intensity analysis [35] of forward and backward propagating pulses, solitary pressure waves in elastic tubes [11] and computational fluid dynamics simulations of local flows [16, 29, 39]. Hybrid (partly analytical, partly numerical) distributed models, which frequently use measurements as inlet conditions, proved to be the most successful on predicting pulse distortions [31]. Sensitivity analysis has also been employed in order to estimate the multiple parameters entering in numerical computations [38]. The need for a detailed examination of the arterial flow, directed also the construction of in vitro silicon replica of the arterial tree [28], which is accompanied by similar hybrid computational tools. Previously, we proposed an analytical, an-harmonic, one-dimensional, viscous model to account for the interdependence between the

peripheral distortion of pressure-flow pulse and physiological-geometrical factors of the arterial tree [52]. Despite the lack of the observed periodicity, this time-domain approach predicted the viscous dissipation of the flow and pressure pulse at remote sites of the arterial network and achieved a quantitative agreement with the systolic peak of the arterial pressure pulse, but failed to fit the diastolic peak and to interpret the initial increase of the systolic peak in the arterial periphery.

The purpose of this study is to extend our pervious analysis, in order to contribute to the interpretation of the initial increase of the systolic peak of the pressure pulse as it propagates away from the heart (and other arterial pulse distortions), through: a careful estimation of all classes of inertial effects (transport and convective acceleration), a physiologically firm constitutive framework for the rheology of blood and the elasticity of the arterial wall, and a three-dimensional, analytical, an-harmonic, time-domain, quasi-lumped model. We name our model *quasi-lumped*, since we represent the arterial network by a single tube (a lump-model analysis characteristic), but the flow dynamics depends an-harmonically on the streamwise space dimension (an unlumped-model analysis characteristic) [55].

In section 2 we illustrate the fluid-structure model, for the interaction between the flow of blood and the elastic response of the arterial wall. The analytical, an-harmonic solution is presented in section 3. A comparison with previous pressure recordings for the radial artery is given in section 4. In the same section we describe the modeling of forward and backward interfering waves and also clarify the role of inertial effects on altering the shape of the arterial pressure, flow, shear stress and radius pulse. In section 5 we discuss the implications of the an-harmonic analysis on interpreting the peripheral distortion of the arterial pulse and therefore correlate inertial effects with arterial dysfunctions like hypertension and atherosclerosis. Finally, some conclusions, possible improvements and extensions of the modeling approach are provided in section 6.

2. **Model.** Blood is a complex fluid (a suspension of deformable cells: red cells, white cells and platelets in an aqueous solution of electrolytes and non-electrolytes: plasma) that flows either in large vessels (systemic arteries and veins), or in a capillary complex network, with rheological properties which vary with pressure, temperature, electromagnetic field and other factors. Computational fluid dynamic simulations can focus on particular branches of the arterial network [16]. Most of these models [39] treat blood as a Newtonian fluid, although its complex, non-Newtonian, rate type character is still a prerequisite [3]. Arteries are inelastic, anisotropic and with a nonlinear stress-strain history [18]. Their material properties may vary along the arterial network, as well as with aging, hypertension innervation, denervation etc. [8, 15, 17, 19, 20, 32, 33]. Pressure recordings have also been used in order to characterize the arterial wall mechanics [27, 50].

In this work we look at the arterial pulse as a traveling wave which satisfies a "wave" equation. The similarities between an-harmonic, time-domain, analytical solutions of the Klein-Gordon equation and the arterial pressure and flow pulse urged us to embody this telegraph wave like equation in an appropriate constitutive framework. Some first results in this direction for a one-dimensional model [52] were promising, but failed to explain thoroughly the distortion of the arterial pulse. This work completes our previous three-dimensional improvements [53, 54]. We concentrate our interest on interpreting the changes in the shape of the arterial pulse as it travels in the arterial network. Nevertheless, the proposed fluid-structure

constitutive model serves as a limiting case to the broadest possible framework for rate type fluids [3, 21, 23, 25] and similar soft tissues [7, 17, 18, 50]. We present an-harmonic, analytical, time-domain, radial symmetric solutions of the coupled fluid-structure wave propagation problem. Although the model geometry corresponds to a flow in a single vessel, the contributions of reflected waves from arterial bifurcations, or stiffer and smaller blood vessels are also included, since the linear character of the model permits expansion of the solution in the eigenfunction space. This is a typical lumped modeling analysis technique. However, our model is not a pure lumped one, since the flow is streamwise space dependent (an un-lumped model analysis characteristic [55]). Therefore, it is legitimate to call our approach a quasi-lumped model.

Henceforth, capital and normal bold characters denote tensors and vectors, respectively, unless otherwise designated. Subscripts a and b, or superscripts (a) and (b) denote variables and constants in the arterial wall and blood, respectively. Characters with over-bars denote dimensionless variables and constants in the arterial wall.

2.1. **The blood flow problem.** We assume that blood is an incompressible, linear viscoelastic, Maxwell fluid, that flows axi-symmetrically, under no temperature gradients, in a single, systemic arterial vessel:

$$\rho_b \frac{D\mathbf{u}}{Dt} = \nabla \cdot \mathbf{T}_b - \nabla P + \mathbf{f}_h, \quad \text{in} \quad \Omega(t), \tag{1}$$

$$\nabla \cdot \mathbf{u} = 0, \quad \text{in} \quad \Omega(t), \tag{2}$$

$$\mathcal{L}\,\mathbf{T}_b = 2\mu_b \mathbf{D}_b, \quad \mathcal{L} \equiv 1 + t_b \frac{\partial}{\partial t}, \tag{3}$$

$$\mathbf{D}_b = \tfrac{1}{2}\left(\mathbf{L}_b + \mathbf{L}_b^T\right), \quad \mathbf{L}_b = \nabla \otimes \mathbf{u}, \tag{4}$$

where

$$\frac{D\mathbf{u}}{Dt} \equiv \frac{\partial \mathbf{u}}{\partial t} + \mathbf{u} \cdot \nabla \mathbf{u} = \frac{\partial \mathbf{u}}{\partial t} - \mathbf{u} \times \boldsymbol{\omega} + \tfrac{1}{2}\nabla u^2 \tag{5}$$

is the material time derivative. P, μ_b, ρ_b, t_b $\mathbf{u}$ and $\boldsymbol{\omega} = \nabla \times \mathbf{u}$ are the blood's, pressure, the shear viscosity, the density, the relaxation time, the velocity vector and the vorticity vector respectively. $\mathbf{f}_h$ is a body force due to the impulsive heart motion. Body force terms, like $\mathbf{f}_h$, are frequently used to fit clinical data [45]. $\mathbf{T}_b$, $\mathbf{L}_b$, $\mathbf{D}_b$ and $\mathbf{I}$ are the viscoelastic stress, the velocity gradient, the rate of deformation and the identity tensors, respectively. Eqs. (1) and (2) are the equations of motion (conservation of momentum) and continuity (conservation of mass for incompressible flow), respectively, which hold in the time dependent domain $\Omega(t)$ (see Fig. 1 and Eq. (12), below). Eq. (3) is the constitutive law for a linear Maxwell fluid. The linear viscoelasticity operator $\mathcal{L}$ is not objective (it changes with the frame of reference). For an objective Maxwell fluid constitutive law, we should replace $\mathcal{L}$ by the material frame indifferent operator $\mathcal{L}_{\mathrm{I}}$, with:

$$\mathcal{L}_{\mathrm{I}}\mathbf{T}_b \equiv \mathbf{T}_b + t_b \overset{\triangledown}{\mathbf{T}}_b, \quad \overset{\triangledown}{\mathbf{T}}_b \equiv \frac{D\mathbf{T}_b}{Dt} - \mathbf{L}_b\mathbf{T}_b - \mathbf{T}_b\mathbf{L}_b^T. \tag{6}$$

$\overset{\triangledown}{\mathbf{T}}_b$ is the upper convective time derivative of $\mathbf{T}_b$. Keeping the frame indifferent form of the constitutive law does not contribute much to the analytical character of the solution, apart from minor modifications, related with the form of $\mathbf{f}_h$ and $P_s(t)$ (see below and in Appendix A). Thereupon, we restrict our analysis to a linear Maxwell

fluid. We assume that the impulsive heart force, $\mathbf{f}_h$, has the typical form of a polar fluid with rotational viscosity [10]:

$$\mathbf{f}_h = \nabla \times \mathbf{A}_h, \quad \mathbf{A}_h = \mathcal{A}_h(r)\, \Psi^{(b)}(t,z)\, \mathbf{e}_\theta. \tag{7}$$

We use cylindrical coordinates (r, θ, z). $\Psi^{(b)}$ is a dimensionless, non-separable, spatiotemporal function. The blood flow is also rotational:

$$\mathbf{u} = \nabla \times \mathbf{A}, \quad \mathbf{A} = \mathcal{A}(r)\, \Psi^{(b)}(t,z)\, \mathbf{e}_\theta\,. \tag{8}$$

$\mathbf{A}$, and $\mathbf{A}_h$, are vector potentials for blood velocity and heart's impulsive force, respectively. $\mathcal{A}$ and $\mathcal{A}_h$ are the radial functions of the above vector potentials, respectively. Notice that we selected $\mathbf{u}$ and $\mathbf{f}_h$ to be collinear and differ only with respect to their radial dependence. Then, the continuity equation for incompressible flow (2) is automatically satisfied. A flow of the form (8) is complex lamellar ($\mathbf{u} \cdot \boldsymbol{\omega} = 0$) [49]. In linearized calculations, only the transient acceleration (the first part of the right hand size of Eq. (5)) survives. Lighthill [24] noticed that almost all pressure gradient combats fluid inertia, and that we are not forced to look towards nonlinear effects, in order to explain the peripheral distortion of the arterial pulse. Accordingly, following an Oseen type approximation, we include the convective acceleration in Eq. (5) as:

$$\mathbf{u} \cdot \nabla \mathbf{u} = -\mathbf{u} \times \boldsymbol{\omega} + \tfrac{1}{2} \nabla u^2 \simeq -\mathbf{u}_c \times \boldsymbol{\omega} + \tfrac{1}{2} \nabla u^2 \tag{9}$$

that is, we retain a linear convection of vorticity term (first term on the right hand side), with $\mathbf{u}_c = u_c\, \mathbf{e}_z$ a constant axial velocity vector, which can be related with vorticity measures [49]. Notice that we left untouched the second, Bernoulli term, of Eq. (9). This quasi-linear insertion of the convective acceleration is vital for our further analysis. It assists the comparison with measured pulses and explains from a new perspective the distortion of the arterial pulse.

2.2. **The arterial wall problem.** A three-dimensional viscoelastic arterial wall model, analogous to the fluid one of Eqs. (1)-(2), is also required. To the best of our knowledge, a complete mathematical analysis of such coupled three-dimensional fluid-structure problems is not available yet [39]. Even in recent, sophisticated, three-dimensional finite element simulations of blood flow in the arterial tree, the structure problem is absorbed into the satisfaction of the boundary conditions for the fluid domain [16, 29, 47]. Simpler models have been proposed to account for stress relaxation of the arterial wall [5, 13, 50, 51]. Of special interest are one-dimensional models, based on the radial deformation, $\boldsymbol{\xi} = \xi(t,z)\, \mathbf{e}_r$ in Fig. 1, of the vessel wall [7, 14, 39]. They are based on the following simplifying assumptions [39]: (i) small vessel thickness ($h \ll R$) in Fig. 1 and plain stresses, (ii) cylindrical reference geometry and radial displacements, (iii) small deformation gradients and (iv) an incompressible arterial wall. We adopt here the approach (and notation) introduced by Canic et al. [7], where the arterial wall is considered a viscoelastic (Kelvin-Voigt), Koiter's type, thin shell, that satisfies, the following one-dimensional equation of motion:

$$\rho_a\, h \frac{\partial^2 \xi}{\partial t^2} - C_1 \frac{\partial^2 \xi}{\partial z^2} - C_2 \frac{\partial^4 \xi}{\partial z^4} + C_0 \xi + D_0 \frac{\partial \xi}{\partial t} - D_1 \frac{\partial^3 \xi}{\partial t \partial z^2} + D_2 \frac{\partial^5 \xi}{\partial t \partial z^4} = f_b, \tag{10}$$

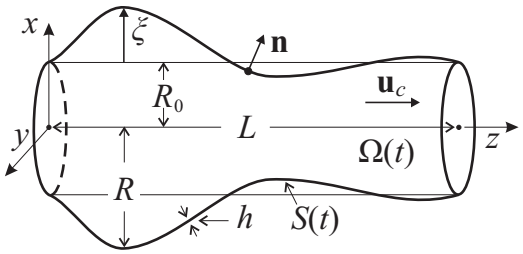

FIGURE 1. Geometry for the deformation of the arterial wall. The deformations, ξ, are radial, with $R = R_0 + \xi$, and R_0 the radius in the reference configuration. The arterial wall is thin, with thickness h. Blood flows along the positive z axis, with mean axial velocity $\mathbf{u}_c$, within the present configuration, $\Omega(t)$, bounded by the the deformed boundary $S(t)$. $\mathbf{n}$ is the normal unit vector on $S(t)$.

where

$$
\begin{aligned}
C_0 &= \frac{h}{R_0^2}\frac{E}{1-\sigma^2}\left(1+\frac{h^2}{12R_0^2}\right)+\frac{P_{\text{ref}}}{R_0},\\
C_1 &= 2\frac{h^3}{12R_0^2}\frac{E\sigma}{1-\sigma^2}, \quad C_2 = \frac{h^3}{12}\frac{E}{1-\sigma^2},\\
D_0 &= \frac{h}{R_0^2}C_v\left(1+\frac{h^2}{12R_0^2}\right),\\
D_1 &= 2\frac{h^3}{12R_0^2}D_v, \quad D_2 = \frac{h^3}{12}C_v,\\
C_v &= \frac{2\lambda_v\mu_v}{\lambda_v+2\mu_v}+2\mu_v, \quad D_v = C_v - 2\mu_v\,.
\end{aligned}
\tag{11}
$$

We embrace the model by Canic et al., because of our further analytical calculations, that exploit the same eigenfunction space, either for the fluid (blood) or the structure (arterial vessel) problem, in sections 3.1 and 3.2 below. C_0, C_1 and C_2 are coefficients that account for elastic effects, while D_0, D_1, D_2, C_v and D_v are coefficients that account for viscoelastic effects. C_0 includes also the effect of prestress, due to the reference pressure P_{ref}, related with circumferential strain [7]. Terms multiplying $h/2$ account for stretching (membrane effects), while terms multiplying $h^3/12$ account for bending (flexural-shell effects) [7]. h is the thickness of the arterial wall and R_0 is the reference, un-deformed radius of the blood vessel at the beginning of the systole phase of the cardiac circle (see Fig. 1). E and σ are the Young's modulus of elasticity and Poisson's ratio, respectively. λ_v and μ_v are the viscoelastic Lame constants and ρ_a the density of the arterial wall.

2.3. **Fluid-structure coupling.** Modeling the interactions between an incompressible blood flow and a deforming vascular structure represents one of the major challenges in the field of cardiovascular mechanics. Appropriate forms of, either the computational domain, or the compatibility, boundary and initial conditions are required. The blood flow problem, of Eqs. (1)-(2), hold in the cylindrical domain:

$$
\Omega(t) = \left\{(r\cos\theta, r\sin\theta, z) \in \mathbb{R}^3 :\, r < R_0 + \xi(t,z),\, \theta \in [0,2\pi],\, z \in [0,L]\right\}, \tag{12}
$$

bounded by the lateral boundary:

$$S(t) = \left\{ (r\cos\theta, r\sin\theta, z) \in \mathbb{R}^3 : \; r = R_0 + \xi(t,z),\; \theta \in [0, 2\pi],\; z \in [0, L] \right\}, \quad (13)$$

which coincides with the viscoelastic membrane that represents the arterial wall, in Fig. 1. The reference configuration corresponds to a straight cylinder with radius R_0 and length L. The coupling between the flow of blood and the vessel wall dynamics is performed through the following kinematic and dynamic boundary conditions:

1. The kinematic condition requiring continuity of velocity:

$$u_r\left(R_0 + \xi(t,z), z, t\right) = \frac{\partial \xi(t,z)}{\partial t}, \quad u_z\left(R_0 + \xi(t,z), z, t\right) = 0. \quad (14)$$

2. The dynamic compatibility condition (10) requiring the balance of fluid (right hand side) and structure (left hand side) forces. f_b is the normal stress that blood exercise on the arterial vessel. Following Canic et. al. [7]:

$$f_b = (1 + \xi/R_0)\sqrt{1 + (\partial\xi/\partial z)^2}\,\mathbf{n} \cdot \left[(P - P_{\text{ref}})\,\mathbf{I} - 2\mu_b \mathbf{D}_b\right] \cdot \mathbf{e}_r, \quad (15)$$

where $\mathbf{n}$ is the normal vector on the deformed lateral boundary $S(t)$ and $\mathbf{e}_r$ is the radial unit vector.

A well posed problem demands inlet-outlet conditions of the form [7]:

1. The pressure is prescribed at both ends:

$$P + P_b - P_c = P_{z=\{0,L\}}(t) + P_{\text{ref}}, \quad \text{at } z = \{0, L\}. \quad (16)$$

2. The blood enters and leaves the single blood vessel parallel to the axis of symmetry, with zero displacement:

$$u_r(t, z = \{0, L\}) = 0, \quad \xi(t, z = \{0, L\}) = 0, \quad u_r \equiv -\mathcal{A}\,\frac{\partial \Psi^{(b)}}{\partial z}. \quad (17)$$

3. The arterial tube is clamped:

$$\frac{\partial \xi}{\partial z}(t, z = \{0, L\}) = 0. \quad (18)$$

Initially, the blood and the arterial wall are at rest, with zero displacement from the reference configuration:

$$\mathbf{u}(t = 0, z) = 0, \;\; \xi(t = 0, z) = 0, \;\; \frac{\partial \xi}{\partial t}(t = 0, z) = 0. \quad (19)$$

Even in its present form, where the arterial vessel is replaced by a thin viscoelastic shell, the fluid-structure problem of Eqs.(1), (2), (10) followed by the boundary conditions (14), (16)-(18) and the initial conditions (19) is a formidable task. A variety of numerical methodologies have been developed to treat similar fluid-structure model, like: finite-element [16], Lattice Boltzmann [29, 43], or heterogeneous domain decomposition methods [39]. Besides, Canic et. al. [7], did not consider the structure problem (10) and (14) (17)-(18) in all its details, but instead applied homogenization methods to derive a reduced model, for numerical evaluation.

The purpose of this study is not to solve a local fluid-structure problem, like the one just presented, but rather to exploit an eigenfunction subspace with anharmonic analytical solutions, in order to interpret changes in a propagating arterial pulse, throughout the arterial network. Hence, the conditions (18)-(19) will be suppressed and the satisfaction of the kinematic conditions on $S(t)$, will be relaxed, by introducing the mean radial displacement ξ_m (see Eq. (55), below).

Eq. (16) is Eq. (3.5) in Ref. [7], augmented with the convective pressure, P_c in Eq. (21), below. The designation of the pressure at the inlet, in Eq. (16), is equivalent with the presence of the impulsive heart force, $\mathbf{f}_h$, in Eq. (7), that defines blood as a polar fluid with rotational viscosity. For numerical investigations the inlet-outlet conditions (16) are preferable, but for our further analytical calculations the presence of $\mathbf{f}_h$ in Eq. (1) is advisable.

3. **Analysis.** In the era of direct numerical simulation in complex geometries [16, 29, 39, 43], and hybrid models, associated with exercise [46], aging [38] or vascular disease [4], analytical solutions, when they exist, they may serve, either as a single theoretical framework for explaining major characteristics of blood flow in arteries, or as suitable input in the above computational methodologies. Most analytical calculations, related to pulse propagation in arteries, rely on Fourier harmonic analysis [30]. The principal drawback of harmonic analysis is that it is limited to the frequency domain and therefore it is impossible to relate specific time events in the cardiac cycle [36]. An an-harmonic, time-domain approach, like the one we introduced in [52], overcomes these defects.

3.1. **The blood flow solution.** After some manipulations of the viscoelastic fluid flow problem consisting of Eqs. (1), (3), (5) and (7)-(9) (for details see Appendix A) we obtain a linear vector telegraph equation:

$$\mu_b \nabla^2 \mathbf{A} - \rho_b \, t_b \, \frac{\partial^2 \mathbf{A}}{\partial t^2} - \rho_b \frac{\partial \mathbf{A}}{\partial t} - \rho_b \, \mathbf{u}_c \cdot \nabla \mathbf{A} + \mathbf{A}_h = \mathbf{0} \,, \tag{20}$$

for the convection and diffusion of vorticity and a generalized Bernoulli equation:

$$P = P_s - P_b + P_c + P_{\text{ref}}, \quad P_b = \tfrac{1}{2} \rho_b \, u^2, \quad P_c = \rho_b \, \mathbf{u}_c \cdot \mathbf{u}, \tag{21}$$

where $P_s = P_s(t)$ is an arbitrary spatial function and P_{ref} is a reference constant pressure. This analytical, nonlinear pressure-flow formula suffices to explain the pulse distortion. Eq. (21) is the cornerstone of all our further calculations, behind the validation of our theoretical approach against experimental recordings. $P_s = P_s(t)$ is a solitary pulse, since it propagates undistorted throughout the arterial network. We attribute its origin, as we did previously and with the body force $\mathbf{f}_h$, to the cardiac output during systole. It may change with the metabolic needs of the body (exercise, relaxation, etc.), or due to cardiac disfunctions (cardiomyopathy, aortic-mitral valve insufficiency, etc.). P_b is the well known Bernoulli's pressure. P_c is the pressure, due to the convection of vorticity (a nonlinear effect that is introduced in our quasi-linear analysis). It emanates from the first term on the right hand side of Eq. (9), while P_b from the second. The form of the cardiac solitary pulse $P_s(t)$, the value of u_c, as well as the amplitude, the width and the shift of the flow pulse $\mathbf{u}$, with respect to P_s, controls all the peripheral changes in the shape of the pressure pulse.

The generalized Bernoulli equation (21) holds in the deformed fluid domain $\Omega(t)$. The inlet-outlet conditions (16) are the special cases of Eq. (21) at $z = \{0, L\}$, with $P_{z=0}(t) = P_s(t)$. Eq. (20) differs from the vorticity equation, only by an arbitrary harmonic vector potential, in the right hand side, which is neglected in our further an-harmonic analysis (for details see Appendix A). This is evident from: (i) the rotational and solenoidal character of $\mathbf{u}$ and $\mathbf{A}$, respectively, in Eq. (8), since $\boldsymbol{\omega} = \nabla \times \mathbf{u} = -\nabla^2 \mathbf{A}$ and (ii) the linear differential operator that acts on the right hand side of Eq.(20).

Let us introduce the dimensionless parameters:

$$\alpha = \mathcal{A}/(L\,u_0),\ \ \alpha_h = \mathcal{A}_h/P_0,\ \ \tilde{r} = r/R_0,\ \ \beta = L/R_0,\ \ p = P/P_0,$$
$$U_c = u_c/u_0,\quad k = U_c/U_b,\ \ U_b = 1/\sqrt{De_b\,Re} = u_b/u_0 = 1/M_b, \tag{22}$$

with

$$u_b = \sqrt{\mu_b/(\rho_b\,t_b)},\quad P_0 = \rho_b\,u_0^2,\quad u_0 = L/t_0. \tag{23}$$

u_b, De_b, M_b, Re, and β, are the shear wave velocity, the Deborah number, the Mach's number, the Reynolds number and the length to radius ratio, respectively. L, t_0, u_0, and P_0, are the characteristic: length, time, velocity and pressure, respectively. We call U_c the convection number. Many, not always equivalent definitions, are given for Deborah number. Some authors even call it Weissenberg number, although under the same name exist other combinations of such parameters [21]. De_b is the ratio of elastic to viscous forces, and U_c is the ratio of convection to inertial forces. Other compositions of De_b, M_b, Re and U_c are also used to describe the physical processes in a Maxwell fluid, like k, the product of Mach's number with the convection number.

If we rescale according to:

$$\tau_b = \varepsilon_b\,t/(2\,De_b\,t_0),\quad \eta_b = \varepsilon_b\,z/(2\,De_b\,L\,U_b),\quad \varepsilon_b = \sqrt{4U_b^2De_b^2\zeta^2 + k^2 - 1}, \tag{24}$$

with τ_b, η_b the dimensionless time and axial coordinates, respectively, and use the transformation:

$$\Psi^{(b)} = e^{(k\eta_b - \tau_b)/\varepsilon_b}\Phi^{(b)}(\tau_b, \eta_b), \tag{25}$$

the vorticity Eq. (20) separates into:

$$\frac{d^2\alpha}{d\tilde{r}^2} + \frac{1}{\tilde{r}}\frac{d\alpha}{d\tilde{r}} + \left(\kappa^2 - \frac{1}{\tilde{r}^2}\right)\alpha = -Re\,\alpha_h(\tilde{r}),\quad \kappa = \zeta/\beta, \tag{26}$$

$$\frac{\partial^2\Phi^{(b)}}{\partial\eta_b^2} - \frac{\partial^2\Phi^{(b)}}{\partial\tau_b^2} - \Phi^{(b)} = 0, \tag{27}$$

where ζ is a dimensionless constant that emanates from the semi-separable form of the blood's velocity vector potential $\mathbf{A}$, in Eq. (8). This is not the first time that the Klein-Gordon Eq. (27) has been used, in order to explain the peripheral distortion of the arterial pulse [6].

After straightforward but lengthy calculations [44], the an-harmonic solution of Eq. (27) can be expressed as:

$$\Psi^{(b)}(\tau_b, \eta_b) = \sum_q c_q^{(b)}\,\Psi_q^{(b)},\quad \Psi_q^{(b)}(\tau_b, \eta_b) \equiv \frac{\partial\psi_q^{(b)}}{\partial\tau_b}, \tag{28}$$

$$\psi_q^{(b)}(\tau_b, \eta_b) = \mathrm{e}^{\frac{k\eta_b - \tau_b}{\varepsilon_b}}\left(\frac{\tau_b - \eta_b}{\tau_b + \eta_b}\right)^{\frac{q}{2}} J_q\left(\sqrt{\tau_b^2 - \eta_b^2}\right), \tag{29}$$

$$\frac{\partial\psi_q^{(b)}}{\partial\tau_b} = \frac{1}{2}\left(\psi_{q-1}^{(b)} - \psi_{q+1}^{(b)} - \frac{2}{\varepsilon_b}\,\psi_q^{(b)}\right), \tag{30}$$

$$-\frac{\partial\psi_q^{(b)}}{\partial\eta_b} = \frac{1}{2}\left(\psi_{q-1}^{(b)} + \psi_{q+1}^{(b)} - \frac{2k}{\varepsilon_b}\,\psi_q^{(b)}\right). \tag{31}$$

J_q is the Bessel function of order q with $\tau_b \geq \eta_b$ and $c_q^{(b)}$ are undetermined constants. We further set $\varepsilon_b > 0$, in order not to use the modified Bessel functions, as in

[52], that limited the quantitative agreement with related measurements. The anharmonic solution (28)-(31) confirms the predictions in [25], that three-dimensional viscoelastic fluid flow solutions decay exponentially as time goes to infinity.

In order to obtain axial velocity profiles of the observed form (see Eqs. (35) and (37) and Fig. 3, below), we assume that the dimensionless radial part of the vector potential $\mathbf{A}_h$ of heart's impulsive force in Eq. (7), is of the form:

$$\alpha_h(\tilde{r}) = p_h \left(\tilde{r}^n + \frac{n^2-1}{\kappa^2}\, \tilde{r}^{n-1} \right), \quad p_h = P_{\rm ref}/P_0, \tag{32}$$

where n is an arbitrary integer. The presence of the reference pressure $P_{\rm ref}$ in Eq. (32) guarantees the equivalence between the present analytical investigation with numerical computations, where inlet-outlet conditions of the form (16) are required. According to the kinematic boundary conditions (14), the axial velocity component vanishes, namely:

$$\alpha_z(\tilde{r}_a) = 0, \quad \alpha_z \equiv \alpha + \alpha/\tilde{r}, \tag{33}$$

in dimensionless form, with:

$$\tilde{r}_a = R/R_0, \quad R = R_0 + \xi(t,z). \tag{34}$$

Then, the solution of Eq. (26) that satisfies the boundary condition (33) is:

$$\alpha(\tilde{r}) = c_r \left[\frac{n+1}{\kappa\, \tilde{r}_a} \frac{J_1(\kappa\, \tilde{r})}{J_0(\kappa\, \tilde{r}_a)} - \left(\frac{\tilde{r}}{\tilde{r}_a} \right)^n \right], \quad c_r = \frac{u_{\rm ref}\, \tilde{r}_a^n}{u_0\, \kappa^2}, \tag{35}$$

where

$$u_{\rm ref} = P_{\rm ref}\, R_0/\mu_b\,, \tag{36}$$

is a reference blood velocity for each arterial vessel. Hence, the axial velocity component becomes:

$$\alpha_z(\tilde{r}) = \frac{(n+1)\, c_r}{\tilde{r}_a} \left[\frac{J_0(\kappa\, \tilde{r})}{J_0(\kappa\, \tilde{r}_a)} - \left(\frac{\tilde{r}}{\tilde{r}_a} \right)^{n-1} \right]. \tag{37}$$

What is measured in related recordings is the volumetric flow rate through the tube, $Q = 2\pi \int_0^R r\, u_z\, d\, r$, with $u_z = u_0\, \alpha_z(\tilde{r})\, \Psi(t,\, z)$. Hence, we define the average flow pulse:

$$\langle u \rangle \equiv Q/(2\pi R_0^2) = u_A\, \Psi^{(b)}, \quad u_A = u_0\, \beta\, \alpha(\tilde{r}_a)/\tilde{r}_a. \tag{38}$$

3.2. **The arterial wall solution.** We can keep terms up to the first order in h, in Eq. (10), if we set:

$$\sigma = \frac{R_0}{h}\, \sigma_0, \quad C_0 \simeq \frac{\gamma\, hE}{R_0^2(1-\sigma^2)}, \quad \gamma \gg 1, \tag{39}$$

that is, the arterial wall is inhomogeneous (the Poisson's ratio depends on the thickness of the arterial wall) which results in:

$$E = \frac{P_{\rm ref} R_0}{\gamma h} \left[1 - \left(\frac{R_0\, \sigma_0}{h} \right)^2 \right], \; C_0 \simeq \frac{P_{\rm ref}}{R_0}, \; C_1 = \frac{P_{\rm ref} \sigma_0 h}{6\gamma}, \; D_0 = \frac{C_v h}{R_0^2}, \tag{40}$$

with C_2, D_1, $D_2 = 0$. Here, γ is a dimensionless constant and σ_0 is the Poisson's ratio, independent of the wall thickness, h. Then Eq. (10) reduces to:

$$\rho_a\, h \frac{\partial^2 \xi}{\partial t^2} - C_1 \frac{\partial^2 \xi}{\partial z^2} + D_0 \frac{\partial \xi}{\partial t} + C_0\, \xi = f_b. \tag{41}$$

This telegraph wave equation is similar to the equivalent vector one (20) for the convection and diffusion of vorticity, and therefore admits similar an-harmonic solution with Eqs. (28)-(31). We introduce the dimensionless parameters:

$$\begin{aligned}
&\tau_a = \varepsilon_a\, t/(\beta_v\, \delta\, \bar{h}\, t_0),\ \ \eta_a = \varepsilon_a z/(L\, U_a \sqrt{\beta_v\, \delta\, \bar{h}}),\ \ \bar{h} = h/L_v,\ \ De_a = t_a/t_0,\\
&U_a = u_a/u_0 = 1/M_a,\ \ \beta_v = L_v/R_0,\ \ \bar{\xi} = \xi/L,\ \ F_b = \beta f_b/(2P_0)\\
&p_s = \beta P_s/(2P_0),\ \ p_{\rm ref} = \beta P_{\rm ref}/(2P_0),\ \ \delta = \rho_a/(2\rho_b),\ \ \varepsilon_a = \sqrt{\bar{h} - 1/4},
\end{aligned} \tag{42}$$

with

$$u_a = \sqrt{\frac{C_1}{2\rho_b R_0}},\quad t_a = \frac{2\rho_b R_0}{D_0},\quad L_v = \frac{D_0\, \rho_a}{C_0}, \tag{43}$$

the wave velocity, the arterial wall relaxation time, and a length constant that depends on viscoelastic parameters of the arterial wall, respectively. $\bar{h}$, $\bar{\xi}$, τ_a and η_a are the dimensionless: arterial wall thickness, axial wall deformation, time and axial coordinate, respectively. M_a and De_a are Mach's and Deborah numbers, respectively, for the arterial wall. δ is a half of densities ratio, β_v is the dimensionless ratio of viscoelastic length to unperturbed vessels radius. p_s and $p_{\rm ref}$ are dimensionless solitary and reference, internal pressures, respectively. Finally, F_b is the dimensionless radial force that blood exerts on the arterial wall. Henceforth, all the calculations are performed under the reasonable approximation that the arterial wall behaves as a polymer solution [48], namely:

$$De_a = 1,\quad \text{or}\quad t_0 = t_a. \tag{44}$$

The solution of Eq. (41) can be decomposed in dimensionless form, as (see Appendix B for the details of the derivation):

$$\bar{\xi}(\tau_a, \eta_a) = \bar{\xi}_s(\tau_a) + \Psi_a(\tau_a, \eta_a) + \Theta(\tau_a, \eta_a), \tag{45}$$

$$\begin{aligned}
\bar{\xi}_s(\tau_a) &= {\rm I}_s(\tau_a) - {\rm I}_s(0) + \varepsilon_a\, p_{\rm ref}\tau_a + \\
&\quad + \varepsilon_a\, ({\rm I}_s'(0) + \varepsilon_a\, p_{\rm ref}) \left(1 - {\rm e}^{\tau_a/\varepsilon_a}\right),
\end{aligned} \tag{46}$$

$${\rm I}_s(\tau_a) = \int\int_0^{\tau_a} {\rm e}^{\tau/\varepsilon_a} p_s(\tau)\, d\tau\, d\tau_a,$$

$$\Psi^{(a)}(\tau_a, \eta_a) = \sum_q c_q^{(a)}\, \Psi_q^{(a)},\ \ \Psi_q^{(a)}(\tau_a, \eta_a) \equiv \frac{\partial \psi_q^{(a)}}{\partial \tau_a}, \tag{47}$$

$$\psi_q^{(a)}(\tau_a, \eta_a) = {\rm e}^{-\frac{\tau_a}{2\varepsilon_a}} \left(\frac{\tau_a - \eta_a}{\tau_a + \eta_a}\right)^{\frac{q}{2}} J_q\left(\sqrt{\tau_a^2 - \eta_a^2}\right), \tag{48}$$

$$\frac{\partial \psi_q^{(a)}}{\partial \tau_a} = \frac{1}{2}\left(\psi_{q-1}^{(a)} - \psi_{q+1}^{(a)} - \psi_q^{(a)}\right), \tag{49}$$

$$-\frac{\partial \psi_q^{(a)}}{\partial \eta_a} = \frac{1}{2}\left(\psi_{q-1}^{(a)} + \psi_{q+1}^{(a)}\right), \tag{50}$$

$$\Theta(\tau_a,\, \eta_a) = \frac{1}{2\varepsilon_a^2} \int_0^{\tau_a} \int_{\eta_a - \tau_a + \tau}^{\eta_a + \tau_a - \tau} {\rm e}^{\frac{\tau}{2\varepsilon_a}}\, H(\tau_a, \eta_a, \tau, \eta)\, d\eta\, d\tau, \tag{51}$$

$$H(\tau_a, \eta_a, \tau, \eta) = \psi_0^{(a)}(\tau_a - \tau, \eta_a - \eta)\, F_d(\tau,\, \eta), \tag{52}$$

$$F_d(\tau,\, \eta) = F_b(\tau,\, \eta) - p_s(\tau) + p_{\rm ref}. \tag{53}$$

The prime in $\mathrm{I}'_s(\tau_a)$ denotes differentiation with respect to the argument. In dimensionless form, the kinematic boundary condition (14) reads:

$$-\alpha(\tilde{r}_a)\,\frac{\partial \Psi^{(b)}(\tau_b,\,\eta_b)}{\partial \eta_b} = \frac{1}{\chi}\,\frac{\partial \bar{\xi}(\tau_a,\,\eta_a)}{\partial \tau_a}, \quad \chi \equiv \frac{\beta_v\,\delta\,\bar{h}\,\varepsilon_b}{2U_b\,De_b\,\varepsilon_a}, \quad \tilde{r}_a = 1+\beta\bar{\xi}. \tag{54}$$

If we substitute Eqs. (28) and (45) into (54), with $\bar{\xi}_s$, $\Psi^{(a)}$, and Θ given by Eqs. (46), (47) and (51), respectively, we obtain an equation that determines the coupling between the blood flow constants $c_q^{(b)}$ and the arterial wall constants $c_q^{(a)}$, as well as the blood flow and arterial wall viscoelastic parameters, in Eqs. (22) and (42), respectively. It is a nonlinear optimization problem, with a lot of information about the nature of the response of the arterial endothelium to the flow of blood.

3.3. **The radial displacement as a blood flow function.** Without solving the nonlinear optimization problem, related with the satisfaction of the kinematic boundary condition (54), useful information about the arterial wall response to the flow of blood is obtained, by examining the inverse problem. More precisely, if the solution to the fluid problem is given, we can integrate Eq. (54) in terms of $\bar{\xi}$:

$$\bar{\xi}(\tau_a,\,\eta_a) = -\chi\,\alpha(\tilde{r}_a)\int \frac{\partial \Psi^{(b)}(\tau_b,\,\eta_b)}{\partial \eta_b}\,d\tau_a, \tag{55}$$

with $\tau_b = \chi\,U_b\,\tau_a$ and $\eta_b = \chi\,U_a\,\eta_a/\sqrt{\beta_v\,\delta\,\bar{h}}$. Here, we silently assumed that $\tilde{r}_a = 1+\beta\,\bar{\xi}_m$, with ξ_m the mean radial displacement of the arterial wall. Similar numerical computations, have also been performed recently [50]. The integral in Eq. (55) can be computed analytically, due to Eq. (28), namely:

$$\int \frac{\partial \Psi^{(b)}}{\partial \eta_b}\,d\tau_a = \frac{1}{\chi\,U_b}\sum_q c_q^{(b)}\,\frac{\partial \psi_q^{(b)}}{\partial \eta}. \tag{56}$$

Mathematical rigor, requires to include an arbitrary function of η_b in the right hand side of (56). Hereafter, we neglect such a spatial dependent term. Finally, substitution of Eq. (56) into Eq. (55) yields:

$$\bar{\xi}(\tau_a,\,\eta_a) = -\frac{\alpha(\tilde{r}_a)}{U_b}\sum_q c_q^{(b)}\,\frac{\partial \psi_q^{(b)}}{\partial \eta_b}. \tag{57}$$

Eq. (57) determines $\bar{\xi}$ in terms of the blood flow eigenfunctions $\psi_q^{(b)}$, as it is the case and for the blood pressure in Eq. (21).

4. **Results.** The emphasis in this study was on developing the general theoretical framework, for interpreting the change in shape of the pulse as it propagates within the arterial tree. Comparison with clinical data will be performed in a future work. Nevertheless, some comparison with sphygmomanometry pressure measurements obtained previously [52], with SphygmoCor Blood Pressure Analysis System, is preformed (see Fig. 2). The SphygmoCor system is accompanied by a transfer functions algorithm [9], that can synthesize the pressure in the aorta (open circles in Fig. 2), from radial artery data (filled circles in Fig. 2). To ease the computations, we assume that the pulse propagates with the same velocity, either in blood or in the arterial wall, namely:

$$u_b = u_a \quad \text{or} \quad \mu_b^{\text{eff}} = h\,P_{\text{ref}}\,\sigma_0\,t_b/\left(12\,R_0\gamma\right). \tag{58}$$

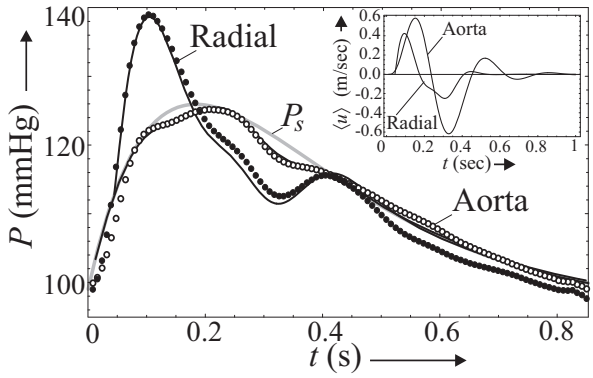

FIGURE 2. The arterial pressure pulse for one cardiac cycle. Aortic (○) and radial (●) pressure pulse measurements from [52]. Gray line: The solitary pulse $P_s(t)$ of Eq. (58). Solid line: The pressure pulse, $P(t, \langle u \rangle)$, of Eq. (21), with $\langle u \rangle$ the average flow pulse in the expansion (60). Enclosed (upper right) the corresponding average flow pulse, with the radial average flow pulse augmented 200 times, to accent its attenuation.

We select $P_s(t)$, approximately, as the convex hull of the aortic pressure pulse (gray line in Fig. 2):

$$P_s(t) = \frac{b_1\, t}{t^2 + t_0^2} + (b_2\, t + b_3\, t^2)\, e^{-t/t_s}, \tag{59}$$

where $t_s = 0.182\,\mathrm{s}$, $b_1 = -6\,\mathrm{mmHg\,s}$, $b_2 = 400\,\mathrm{mmHg/s}$, $b_3 = 100\,\mathrm{mmHg/s^2}$, and t_0 as t_a in Table 1, due to Eq. (44).

4.1. **Modeling wave reflections from arterial junctions.** Essential elements for decoding the peripheral distortion of the arterial waveform are reflected waves, emanating from bifurcations in the arterial tree, or possible abnormalities in the structure of the arterial vessel. For the blood flow in a single arterial vessel of Fig. 1 these factors seem not to be in the picture. However, our model is quasi-lump, and the interference of forward and reflected propagating waves enter through, either the eigenfunction expansion of the solution in Eqs. (28) and (47), or the material parameters and geometric factors of the arterial segments, that vary from one segment to the next. Moreover, segmentation methods like those developed previously [52] can also be applied, but they will not be considered here.

In order to accent the adaptability of our an-harmonic approach to fit the pressure waveform, we used up to three terms in the expansion of Eq. (28):

$$\langle u \rangle = \sum_{i=1}^{3} c_i\, \langle u \rangle^i = c_1\, \langle u \rangle^F + c_2\, \langle u \rangle^{R_1} + c_3\, \langle u \rangle^{R_2}, \tag{60}$$

with $\langle u \rangle^F$ the forward flow pulse and $\langle u \rangle^{R_i}$, $i = 1, 2$, the reflected flow pulses from the arterial periphery. Every term in Eq. (60) has a clear physical meaning: $\langle u \rangle^F$ is the initial forward flow pulse due to cardiac outflow and $\langle u \rangle^{R_i}$, $i = 1, 2$, are the reflected flow pulses which originate from bifurcations or stiffer parts of the peripheral arterial network. Each one of the reflected waveforms stands for the

TABLE 1. Material and geometrical parameters.

	Units	Aorta	Radial		
			$\langle u\rangle^F$	$\langle u\rangle^{R_1}$	$\langle u\rangle^{R_2}$
κ		1	1	1	1
n		3	3	3	3
q		4	4	2.25	16
$c_i \times 10^{-4}$		185.6	74.7	1.7	959566
σ_0		0.3	0.3	0.3	0.3
$\gamma \times 10^{-5}$		101.3	50.6	50.6	7.7
t_0	(s)	1	1	1	1
t_a	(s)	1	1	1	1
$t_b \times 10^{-2}$	(s)	8	4	4	1.5
L	(m)	1	2	2	2
h	(mm)	0.5	0.5	0.5	0.5
z	(cm)	5	40	40	40
ξ_m	(mm)	1	1	1	1
R_0	(mm)	10	4	4	4
P_{ref}	(mmHg)	99	99	99	99
$\rho_b \times 10^{-3}$	(Kgr/m)	1	1	1	1
u_c	(cm/s)	0.05	78.5	78.5	78.5

particular site of the arterial network from where it emerges, in terms of geometrical or physiological parameters that are involved (see Table 1). It may represent a single bifurcation, or the accumulative effect of a sub-network of the arterial tree.

All *geometrical parameters*, like: (i) the thickness of the arterial wall, h, (ii) the length L, and (iii) the reference radius, R_0, of the vessel, (iv) the axial position of the pulse, z, (v) the mean radial displacement, ξ_m, and all *material parameters*, like: (i) the viscoelastic time constants, t_b, t_a, for blood and the arterial wall, respectively, (ii) the Poisson's ratio, σ_0, (iii) the density of blood, ρ_b, (iv) the reference pressure, P_{ref} and (v) the mean axial blood velocity, u_c, have regular values in Table 1, for a Maxwell type blood flow in a Kelvin-Voigt viscoelastic arterial vessel. Nevertheless, the dimensionless parameter γ is in fact an effective parameter that satisfies Eq. (58), and therefore violates the constrain $\gamma \gg 1$, of Eq. (39), in Table 1. Moreover, ξ_m is not really a geometrical parameter at all, since in a more rigorous calculation is derived from the mean value of deformations (57), that meet the expansion (60).

Since related flow data are not available to us, the forward flow pulse, $\langle u\rangle^F$, was enough to fit the pressure pulse for the aorta (the fitting curve is almost covered from the open circles in Fig. 2), while for the radial artery sufficed two additional flow pulses, $\langle u\rangle^{R_i}, i = 1, 2$, that originate, from reflection in the periphery. The time shift $t \sim 0.15\,\text{s}$ to the right, for the systolic peak in the aorta, compared to that of the radial artery, does not correspond to a pure wave propagation phenomenon and is usually attributed to the interference of the forward pressure pulse with a reflected one from the arterial periphery, that boosts pressure in early diastole [30]. This distortion of the pressure pulse of the aorta results in an inflection point at $t \sim 0.15\,\text{s}$ (see Fig. 2), which is interrelated with a measure of the distortion, the augmentation index [30].

According to measurements [24], the pulse wave velocity, u_a, increases in the arterial periphery about two times the values for the aorta ($\sim 5\,\text{m/sec}$). It is confirmed

TABLE 2. Derived effective material parameters.

	Units	Aorta	Radial		
			$\langle u\rangle^F$	$\langle u\rangle^{R_1}$	$\langle u\rangle^{R_2}$
μ_b	(Kgr/(m s))	1300	3250	3250	8000
C_1	(N/m)	325	650	650	4267
$u_{\rm ref}$	(cm/s)	10	1.6	1.6	0.7
u_a	(m/s)	4	9	9	23

from the tabulated values in Table 2, except the third term in Eq. (60). However, such deviations are justified, since, as we mentioned previously, the reflected waves may represent the accumulative effects of one or even more arterial branches in our quasi-lumped model analysis. Notice that $u_c \sim 0$ for the aorta, in Table 1 and in all cases $u_c < u_a$. The t_b values of Table 1 correspond to a viscoelastic fluid with Deborah's number, between that of industrial oil ($\mathrm{De}_b \sim 10^{-3}$), and polymer solution ($\mathrm{De}_b \sim 1$) [48]. The reference blood velocity, $u_{\rm ref}$, in Table 2 has typical values for, either large arteries (aorta) and arterioles (the forward and first reflected pulse), or capillaries (the second reflected pulse). The flow pulse (60) still retains properties that appeared and in previous studies [52, 54], namely it is a relatively undistorted waveform (a *quasi-solitary* wave), since it maintains its shape although it attenuates (due to viscous dissipation), as it propagates away from the heart (increasing z).

4.2. **Velocity profiles and modeling disfunction in terms of u_c.** Velocity profiles are given in Fig. 3. The parameter κ remains arbitrary. Hence, it may serve

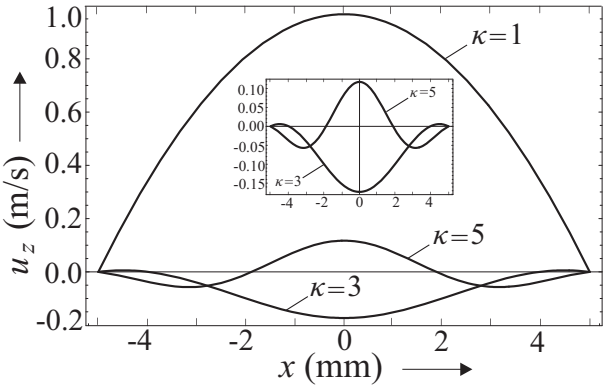

FIGURE 3. Axial velocity profiles for varying κ, at the systolic peak ($\Psi(t,\, z) = \Psi_{\max} = 2 \times 10^{-3}$). All other parameters are the same with those in Tables 1 and 2 for the radial artery. In the enclosed figure a magnification of the region for $\kappa = 3$ and 5 is given.

as a fitting parameter for related recorded profiles. For values of u_c intermediate to the aortic ($u_c = 5\,\mathrm{cm/s}$) and the radial ($u_c = 8\,\mathrm{m/s}$) pressure pulse, the diastolic peak may disappear, as it is evident from Fig. 4. This is the case for patients with hypertension and arteriosclerosis, but with a higher systolic peak than that of the $u_c = 5\,\mathrm{m/s}$ curve in Fig. 4, due to an additional reflection from a stiffer part of the

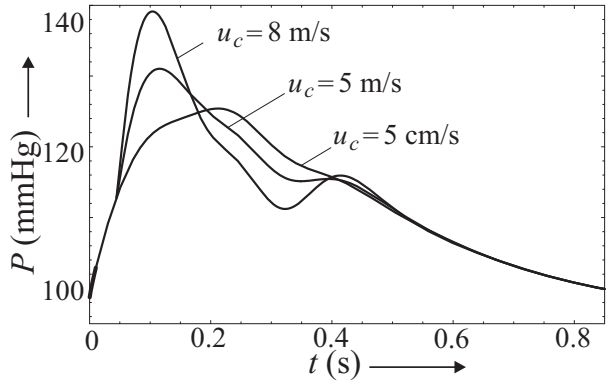

FIGURE 4. The pressure pulse for varying mean axial blood velocity constant u_c. All other material parameters are the same with those in Fig. 2 and Tables 1and 2, for the radial artery. The diastolic peak disappears for $u_c = 5\,\mathrm{m/s}$.

arterial network (higher pulse wave velocity, or smaller t_b in the enclosed figure in Fig. 2), that boosts pressure in late systole [34].

4.3. **Wall shear stress and radius pulses.** One of the principal factors, related with arterial disease, is the wall shear stress [22]:

$$\tau_s^{(b)} = \mu_b \frac{\partial u_z}{\partial r}, \quad \text{on} \quad S(t): \quad r = R_0 + \xi(t,z), \tag{61}$$

where $u_z = u_0\,\alpha_z(r)\,\Psi^{(b)}(t,z)$. The wall shear stress pulse is depicted in Fig. 5 for varying the mean axial blood velocity, u_c, related to convection effects. It is of the

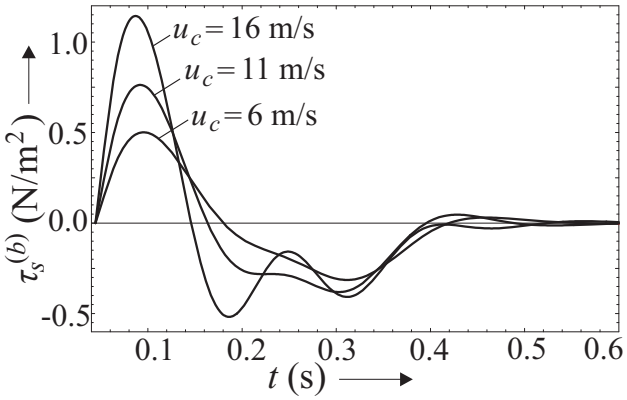

FIGURE 5. The arterial wall shear stress pulse $\tau_s^{(b)}$ for varying u_c, where $\nu_{\mathrm{eff}} = 4.6 \times 10^{-6}\mathrm{m}^2/s$ and $u_h = 50\,\mathrm{cm/s}$. All other parameters, except Ψ, are the same with those in Fig. 2, for the radial artery.

correct order and shape found in the literature [12]. The radius displacement pulse is shown in Fig. 6 also for varying u_c, calculated using Eqs. (34) and (57). Higher

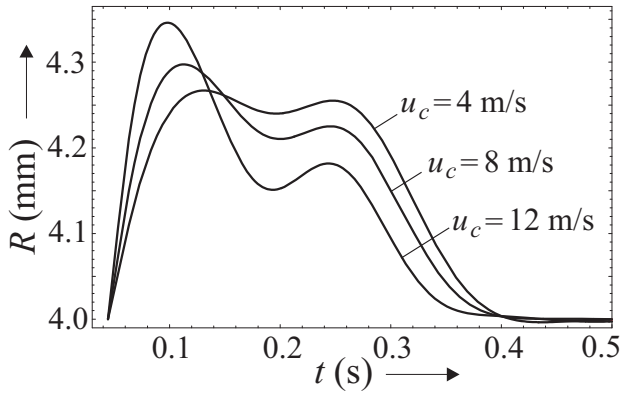

FIGURE 6. The radius displacement pulse for varying u_c. All other parameters (except u_h which is the same with that in Fig. 2) are the same with those in Fig. 5.

u_c values result in steepening of the "systolic" peak in both the wall shear stress and the radius pulses, as expected. Notice that for $u_c = 16\,\mathrm{m/s}$, the "diastolic" valley ($0.15\,\mathrm{s} \leq t \leq 0.4\,\mathrm{s}$) of the the wall shear stress pulse in Fig. (5), deforms dramatically. Moreover, for $u_c = 4\,\mathrm{m/s}$ in Fig. 6 (close to $u_c = 5\,\mathrm{m/s}$ in Fig. 4, which corresponds to the disappearance of the diastolic peak), there is an equilibration of the "systolic" and "diastolic" peaks. Such theoretical estimates require close inspection and await confirmation from real data, for patients with vascular disease (hypertension, atherosclerosis, etc.).

5. **Discussion.** The promising but insufficient results of our previous work [52] and the enlightening review on arterial fluid dynamics by Pedley [36], exhorted us to read the pulse propagation theory, by the eminent fluid dynamist Lighthill [24]. Therein, Sir James Lighthill remarks: (a) *"Almost all the pressure gradient goes into acceleration, that is, into combating the inertia of the fluid"* [chapter 10, page 206] and (b) *"This means that we are not forced to look towards nonlinear effects to explain this waveform change"* [chapter 12, page 250]. Both of them motivated and formed the present analysis.

One-dimensional wave [15], and wave like equations [6], are frequently used to describe the peripheral distortion of the arterial pulse. However, they originate from qualitative postulates and they are not based on a firm constitutive framework. In contrary, in this work, even though the three-dimensional Klein-Gordon telegraph wave Eq. (20) is analogous to the one-dimensional one [6], it emanates from an appropriately constructed viscoelastic, fluid-structure constitutive model. Caflisch et al. [6] neglected the inertial convective term (9). In contrary, herein, the Oseen type approximation in Eq. (9) includes all types for inertial effects and results in the analytical pressure-flow relation (21), which plays a decisive role on the interpretation of the peripheral distortion of the arterial pulse. Lately, Roper and Brenner [42] discussed the usefullness of the linearized Navier-Stokes equations,

according to the Oseen approximation (9), in fluid dynamics. Besides, the analytical, an-harmonic solutions of Eqs. (28)-(31) and Eq. (35) satisfy recent existence [23] and time-decay [25] theorems for general three-dimensional viscoelastic flows.

Recently, time-domain models have been proposed, to account for the distortion of the pulse in systemic arteries [1, 2]. Usually, the initial increase of the systolic peak of the pressure pulse, far away from the heart, is attributed to close type of wave reflections in small peripheral vessels [30]. This observation can be integrated in our quasi-lumped model, if we moreover permit to the mean axial flow velocity parameter $\mathbf{u}_c$ to represent and such factors (as we mention in Appendix A). However, the theoretical analysis of section 4 interprets this initial increase through the pure inertial origin of $\mathbf{u}_c$: it is related with the convection of vorticity and therefore with possible associated disturbances, even turbulence, in blood flow. In particular, when $2\mathbf{u}_c \ll \mathbf{u}$, the Bernoulli pressure, P_b (changes in the magnitude, u, of the flow pulse), dominates the shape of the pulse in Eq. (21) and the pressure pulse for the aorta is given as:

$$P_{\text{aorta}} \simeq P_s(t) - P_b, \quad P_b = \tfrac{1}{2}\rho_b\, u^2\,. \tag{62}$$

Otherwise, when $2\mathbf{u}_c \gg \mathbf{u}$, the convective pressure, P_c, prevails and the pressure pulse for a peripheral arterial vessel (radial artery, etc.), is given as:

$$P_{\text{radial}} \simeq P_s(t) + P_c, \quad P_c = \rho_b\, \mathbf{u}_c \cdot \mathbf{u}\,. \tag{63}$$

The inner product in the above equality for P_c denotes the deviation of the blood flow velocity $\mathbf{u}$ from the mean axial flow velocity $\mathbf{u}_c$ and therefore the convection of vorticity. The form of the pressure pulse, computed from Eqs. (62-63), depends always on the shape, as well as the amplitude, the width and the shift of the flow pulse, with respect to P_s. Notice the minus and plus signs in front of the Bernoulli pressure, P_b, and the convective pressure, P_c, in Eqs. (62) and (63), respectively, which have the dramatic effect on the shape of the pressure pulse in Fig. 2.

Whereas the agreement of the theory (Eqs. (62-63)) with sphygmomanometry pressure measurements is quantitative in Fig. 2, the estimated average aortic flow pulse (in the enclosed figure in Fig. 2) does not necessarily match similar velocimetry recordings. This is because, as we mentioned earlier, we fitted pressure data without having available simultaneous flow recordings. Therefore, in order to stress the flexibility of our analytical, an-harmonic methodology we selected just one term in the eigenfunction expansion (28) for the aorta. This can easily be improved with suitable, even more, terms in the eigenfunction expansion (28) or (60). In a future work, where we will validate our theory against simultaneous in-vivo pressure-flow pulse monitoring, for patients under pharmacological treatment, more terms in the expansion (28) or (60) will be required.

Nevertheless, the flow pulse, either of the correct (radial artery) or of the approximate form (aorta) of the enclosed figure in Fig. 2, can be very advantageous on interpreting useful features of the pressure pulse, like: the diastolic and systolic peak, the augmentation index, the dicrotic notch, etc., from a quite different perspective. More precisely, in the case of the aortic pressure pulse, the square of the systolic peak of the flow pulse is proportional to the augmentation index, since we selected P_s as the convex hull of the aortic pressure pulse, due to the positive definite character of the Bernoulli's pressure P_b and the minus sign in Eq. (62). Similarly, for the radial artery (or any other peripheral vessel with similar waveform), the peak of the total (forward and reflected) flow pulse is proportional to the systolic peak of the pressure pulse. In this case the pressure pulse is approximately given

by Eq. (63) and the convective pressure P_c depends on the sign of the flow pulse $\mathbf{u}$, since $\mathbf{u}_c$ is defined as a positive constant. Then, the plus sign in Eq. (63) results either in the initial increase of the systolic peak in Fig. 2 or the appearance (or disappearance, for a suitable value of u_c) of the diastolic peak in Fig. 4, although the flow pulse suffers viscous dissipation (see Fig. 8.1 in [30] and [52, 54]).

Because recorded pulses are blood-borne mediators of energy transfer, a wave pattern can inform us about all the mechanical factors that influence the pressure or flow. As an example, in disease like hypertension, reflected waves are of central importance, since they arrive early due to an increased pulse wave velocity. Therefore, adjusting such parameters in our model will contribute to a better understanding of such cardiovascular diseases. Moreover, low wall shear stress is known to lead to the development and progression of atherosclerotic plaque culminating in high-risk vulnerable plaque likely to rupture and cause an acute embolic event. The magnitude of the systolic peak of the wall shear stress, in combination with systemic and or genetic risk factors, like hyperlipidemia, determines the natural history of each plaque. Therefore, a methodical comparison between computed wall shear stress and radius pulses like those in Figs. 5 and 6, respectively, and possible available in vivo data is required. Only then the role of principal factors, like $\mathbf{u}_c$, on altering the shape of the pulse will be evaluated and become a tool in clinical practice for hypertension, atherosclerosis, coronary artery disease, diabetes, etc.

6. **Conclusions.** The primary goal of this work was to exploit the an-harmonic function space introduced in our previous work, in order to interpret the peripheral distortion of the arterial pressure, flow, radius and wall shear stress pulse. A proper viscoelastic fluid-structure constitutive framework was developed, that resulted in a wave like telegraph equation for the convection and diffusion of vorticity. With the aid of an Ossen type approximation for the material derivative, that introduces a mean axial velocity parameter, $\mathbf{u}_c$, the quasi-lumped model takes also into account all types of inertial effects (temporal, transport and convective acceleration). The reflected waves from the arterial periphery, enter in our analysis, either directly, through specific terms in the eigenfunction expansion, or indirectly, through the value of $\mathbf{u}_c$. We derived a generalized Bernoulli equation for the pressure-flow interdependence. Close to the aorta the Bernoulli pressure, P_b, dominates the flow. At larger distances from the heart, the convection of vorticity, P_c, related with higher $\mathbf{u}_c$ values, is responsible, either for the increase of the systolic peak, or for the emergence of the diastolic peak. Far away from the heart, blood's viscosity is responsible either for the final, or the continuous attenuation of the pressure and flow (as well as radius and wall shear stress) pulse, respectively. The interplay between the form of the cardiac in origin solitary pulse P_s, the value of $\mathbf{u}_c$ and physiological and geometrical factors that act on the amplitude, the width and the shift of the flow pulse with respect to P_s, account for irregularities in the shape of the pressure pulse. Besides, the parameter $\mathbf{u}_c$, can serve and as a clinical indicator for cardiovascular diseases.

A more detailed picture of the capabilities and limitations of the modeling approach will be provided only after solving the nonlinear optimization problem, corresponding to the kinematic boundary condition on the arterial wall. The proposed fluid-structure model can also be coupled with Maxwell's equations, in a complete electro-hydro-elasto-dynamic framework, in order to interpret measured electrical impedance cardiography waveforms on the thorax. A validation of the model against

simultaneous invasive flow-pressure recordings, for patients under pharmacological treatment is also under investigation.

Acknowledgments. We would like to thank the anonymous referees for their comments and suggestions, which significantly improved the quality of the paper. The first author acknowledges helpful discussions with A.B. Shvartsburg, during early stages of this work.

REFERENCES

[1] J. Alastruey, K. H. Parker, J. Peiró and S. J. Sherwin, *Analysing the pattern of pulse waves in arterial networks: A time-domain study*, J. Engrg. Math., **64** (2009), 331–351.
[2] J. Alastruey, *On the mechanics underlying the reservoir-excess separation in systemic arteries and their implications for pulse wave analysis*, Cardiovasc. Eng., **10** (2010), 176–89.
[3] M. Anand and K. R. Rajagopal, *A shear thinning viscoelastic fluid model for describing the flow of blood*, Inter. J. Cardiovasc. Med. Science, **4** (2004), 59–68.
[4] M. C. Aoi, C. T. Kelley, V. Novak and M. S. Olufsen, *Optimization of a mathematical model of cerebral autoregulation using patient data*, in "Proceedings of the 7$^{\text{th}}$ IFAC Symposium on Modelling and Control in Biomedical Systems," Vol. 7, (2009), 181–186.
[5] D. Bessems, C. C. Giannopapa, M. C. M. Rutten and F. N. van de Vosse, *Experimental validation of a time-domain based wave propagation model of blood flow in viscoelastic vessels*, J. Biomech., **41** (2008), 284–291.
[6] R. Caflisch, G. Majda, C. Peskin and G. Strumolo, *Distortion of the arterial pulse*, Math. Biosci., **51** (1980), 229–260.
[7] S. Čanić, J. Tambača, G. Guidoboni, A. Mikelić, C. J. Hartley and D. Rosenstrauch, *Modeling viscoelastic behavior of arterial walls and their interaction with pulsatile blood flow*, SIAM J. Appl. Math., **67** (2006), 164–193.
[8] L. Cardamone, A. Valentin, J. F. Eberth and J. D. Humphrey, *Origin of axial prestretch and residual stress in arteries*, Biomechan. Model. Mechanobiol., **8** (2009), 431–446.
[9] C. H. Chen, E. Nevo, B. Fetics, P. H. Pak, F. C. P. Yin, W. L. Maughan and D. A. Kass, *Estimation of central aortic pressure waveform by mathematical transformation of radial tonometry pressure: Validation of generalized transfer function*, Circulation, **95** (1997), 1827–1836.
[10] S. C. Cowin, *Polar fluids*, Physics of Fluids, **11** (1968), 1919–1927.
[11] E. Crépeau and M. Sorine, *A reduced model of pulsatile flow in an arterial compartment*, Chaos Soliton Fractals, **34** (2007), 594–605.
[12] G. Dai, M. R. Kaazempur-Mofrad, S. Natarajan, Y. Zhang, S. Vaughn, B. R. Blackman, R. D. Kamm, G. Garcia-Cardena and M. A. Gimbrone, Jr., *Distinct endothelial phenotypes evoked by arterial waveforms derived from atherosclerosis-susceptible and -resistant regions of human vasculature*, Proc. Nat. Acad. Sci., **101** (2004), 14871–14876.
[13] K. DeVault, P. A. Gremaud, V. Novak, M. S. Olufsen, G. Vernières and P. Zhao, *Blood flow in the circle of Willis: Modeling and calibration*, Multiscale Model. Simul., **7** (2008), 888–909.
[14] J. Filo and A. Zaušková, *2D Navier-Stokes equations in a time dependent domain with Neumann type boundary conditions*, J. Math. Fluid Mech., **12** (2010), 1–46.
[15] Y. C. Fung, "Biomechanics, Mechanical Properties of Living Tissues," Springer-Verlag, New York, 1993.
[16] L. Grinberg, T. Anor, E. Cheever, J. R. Madsen and G. E. Karniadakis, *Simulation of the human intracranial arterial tree*, Phil. Trans. R. Soc. A, **367** (2009), 2371–2386.
[17] G. A. Holzapfel, T. C. Gasser and M. Stadler, *A structural model for the viscoelastic behavior of arterial walls: Continuum formulation and finite element analysis*, Eur. J. Mech. Solids, **21** (2002), 441–463.
[18] G. A. Holzapfel, T. C. Gasser and R. W. Ogden, *A new constitutive framework for arterial wall mechanics and a comparative study of material models. Soft tissue mechanics*, J. Elast., **61** (2000), 1–48.
[19] G. A. Holzapfel and R. W. Ogden, *Constitutive modelling of passive myocardium: A structurally based framework for material characterization*, Phil. Trans. R. Soc. A, **367** (2010), 3445–3475.

[20] J. D. Humphrey and C. A. Taylor, *Intracranial and abdominal aortic aneurysms: Similarities, differences and need for a new class of computational models*, Ann. Rev. Biomed. Eng., **10** (2008), 221–246.
[21] D. D. Joseph, M. Renardy and J.-C. Saut, *Hyperbolicity and change of type in the flow of viscoelastic fluids*, Arch. Rat. Mech. Anal., **87** (1985), 213–251.
[22] D. K. Ku, D. P. Giddens, C. K. Zarins and S. Glagov, *Pulsatile flow and atherosclerosis in the human carotid bifurcation. Positive correlation between plaque location and low oscillating shear stress*, Arteriosclerosis, **5** (1985), 293–302.
[23] Z. Lei, C. Liu and Y. Zhou, *Global solutions for incompressible viscoelastic fluids*, Arch. Rat. Mech. Anal., **188** (2008), 371–398.
[24] J. Lighthill, "Mathematical Biofluiddynamics," Based on the lecture course delivered to the Mathematical Biofluiddynamics Research Conference of the National Science Foundation held from July 1620, 1973, at Rensselaer Polytechnic Institute, Troy, New York, Regional Conference Series in Applied Mathematics, No. 17, SIAM, Philadelphia, Pa., 1975.
[25] F. Lin and P. Zhang, *On the initial-boundary value problem of the incompressible viscoelastic fluid system*, Commun. Pure Appl. Math., **61** (2008), 539–558.
[26] M. Lopez de Haro, J. A. P. del Rio and S. Whitaker, *Flow of Maxwell fluids in porous media*, Transport in Porous Media, **25** (1996), 167–192.
[27] I. Masson, P. Boutouyrie, S. Laurent, J. D. Humphrey and M. Zidi, *Characterization of arterial wall mechanical behavior and stresses from human clinical data*, J. Biomech., **41** (2008), 2618–2627.
[28] K. S. Matthys, J. Alastruey, J. Peiro, A. W. Khir, P. Segers, P. R. Verdonck, K. H. Parker and S. J. Sherwin, *Pulse wave propagation in a model human arterial network: Assessment of 1-D numerical simulations against in vitro measurements*, J. Biomech., **40** (2007), 3476–3486.
[29] S. Melchionna, M. Bernaschi, S. Succi, E. Kaxiras, F. J. Rybicki, D. Mitsouras, A. U. Coskun and C. L. Feldman, *Hydrokinetic approach to large-scale cardiovascular blood flow*, Comput. Phys. Comm., **181** (2010), 462-472.
[30] W. W. Nichols and M. F. O'Rourke, "McDonald's Blood Flow in Arteries," Arnold Publishers, London, 1998.
[31] M. S. Olufsen, C. S. Peskin, W. Y. Kim, E. M. Pedersen, A. Nadim and J. Larsen, *Numerical simulation and experimental validation of blood flow in arteries with structured tree outflow conditions*, Ann. Biomed. Eng., **28** (2000), 1281–1299.
[32] R. W. Ogden, "Nonlinear Elastic Deformations," 2^{nd} edition, Dover Publications, Inc., Mineola, New York, 1997.
[33] R. W. Ogden and G. Saccomandi, *Introducing mesoscopic information into constitutive equations for arterial walls*, Biomechan. Model. Mechanobiol., **6** (2007), 333–344.
[34] M. F. O'Rourke and J. Hashimoto, *Mechanical factors in arterial aging: A clinical perspective*, J. Amer. Coll. Cardiol., **50** (2007), 1–13.
[35] K. H. Parker, *An introduction to wave intensity analysis*, Med. Biol. Eng. Comput., **47** (2009), 175–188.
[36] T. J. Pedley, *Mathematical modelling of arterial fluid dynamics. Mathematical modelling of the cardiovascular system*, J. Engrg. Math., **47** (2003), 419–444.
[37] A. D. Polyanin, "Handbook of Linear Partial Differential Equations for Engineers and Scientists," Chapman & Hall/CRC, Boca Raton, Florida, 2002.
[38] S. R. Pope, L. M. Ellwein, C. L. Zapata, V. Novak, C. T. Kelley and M. S. Olufsen, *Estimation and identification of parameters in a lumped cerebrovascular model*, Math. Biosci. Eng., **6** (2009), 93–115.
[39] A. Quarteroni, *Cardiovascular mathematics*, in "International Conference on Mathematics," Vol. I, Eur. Math. Soc., Zürich, (2007), 479–512.
[40] R. Quintanilla and K. R. Rajagopal, *On Burgers fluids*, Math. Meth. Appl. Sci., **29** (2006), 2133–2147.
[41] E. A. Rosei, G. Mancia, M. F. O'Rourke, M. J. Roman, M. E. Safar, H. Smulyan, J. G. Wang, I. B. Wilkinson, B. Williams and C. Vlachopoulos, *Central blood pressure measurements and antihypertensive therapy*, Hypertension, **50** (2007), 154–160.
[42] M. Roper and M. P. Brenner, *A nonperturbative approximation for the moderate Reynolds number Navier-Stokes equations*, Proc. Nat. Acad. Sci. USA, **106** (2009), 2977–2982.
[43] F. J. Rybicki, S. Melchionna, D. Mitsouras, A. U. Coskun, A. G. Whitmore, M. Steigner, L. Nallamshetty, F. G. Welt, M. Bernaschi, M. Borkin, J. Sircar, E. Kaxiras, S. Succi, P. H. Stone and C. L. Feldman, *Prediction of coronary artery plaque progression and potential*

rupture from 320-detector row prospectively ECG-gated single heart beat CT angiography: Lattice Boltzmann evaluation of endothelial shear stress, Int. J. Cardiovasc. Imaging, **25** (2009), 289–299.

[44] A. B. Shvartsburg, "Impulse Time-Domain Electromagnetics of Continuous Media," Birkhäuser Boston, Inc., Boston, MA, 1999.

[45] J. Stalhand, *Determination of human arterial wall parameters from clinical data*, Biomechan. Model. Mechanobiol., **8** (2009), 141–148.

[46] B. N. Steele, M. S. Olufsen and C. A. Taylor, *Fractal network model for simulating abdominal and lower extremity blood flow during resting and exercise conditions*, Comp. Meth. Biomech. Biomed. Eng., **10** (2007), 39–51.

[47] C. A. Taylor and C. A. Figueroa, *Patient-specific modeling of cardiovascular mechanics*, Annu. Rev. Biomed. Eng., **11** (2009), 109–134.

[48] N. Phan-Thien, "Understanding Viscoelasticity. Basics of Rheology," Advanced Texts in Physics, Springer-Verlag, Berlin, 2002.

[49] C. Truesdell, "The Kinematics of Vorticity," Indiana Univ. Publ. Sci. Ser. no. 19, Indiana University Press, Bloomington, 1954.

[50] D. Valdez-Jasso, H. T. Banks, M. A. Haider, D. Bia, Y. Zocalo, R. L. Armentano and M. S. Olufsen, *Viscoelastic models for passive arterial wall dynamics*, Adv. Appl. Math. Mech., **1** (2009), 151–165.

[51] D. Valdez-Jasso, M. A. Haider, H. T. Banks, D. B. Santana, Y. Z. German, R. L. Armentano and M. S. Olufsen, *Analysis of viscoelastic wall properties in ovine arteries*, IEEE Trans. Biomed. Eng., **56** (2009), 210–219.

[52] P. A. Voltairas, D. I. Fotiadis, C. V. Massalas and L. K. Michalis, *Anharmonic analysis of arterial blood pressure and flow pulses*, J. Biomech., **38** (2005), 1423–1431.

[53] P. A. Voltairas, D. I. Fotiadis and L. K. Michalis, *An-harmoninc analysis of the arterial pulse*, in "Advanced Topics in Scattering and Biomedical Engineering," World Scientific Publ., Hackensack, NJ, (2008), 380–387.

[54] P. A. Voltairas, D. I. Fotiadis, A. Charalambopoulos and L. K. Michalis, *An-harmonic modeling of the peripheral distortion of the arterial pulse*, in the e-book "Single and Two-Phase Flows on Chemical and Biomedical Engineering" (eds. R. Lima and R. Dias), Bentham Science Publishers, in press.

[55] M. Zamir, "The Physics of Coronary Blood Flow," With a foreword by Y. C. Fung, Biological and Medical Physics, Biomedical Engineering, Springer, New York, AIP Press, New York, 2005.

Appendix A. **The generalized Bernoulli's equation.** Mathematically, Eq. (9) implies that $\mathbf{u}_c \sim \mathbf{u}$. In our quasi-lumped model we will deviate from this approximation. Although, from Eq.(9), $\mathbf{u}_c$ takes into account the convection of vorticity (the second term on the right hand side), we will additionally assume that $\mathbf{u}_c$, indirectly, takes also into account physiological factors that are left out from a viscoelastic fluid flow in an infinite, viscoelastic thin shell of circular cross section, like: the flow geometry (large and small vessels, bifurcations, etc.), cardiac or other circulatory disfunctions in blood flow, the gradual taper of arteries with distance from the heart (a term that encompasses both a reduction in cross sectional area and an increase in stiffness), etc. Hence, $\mathbf{u}_c$ serves as an effective parameter of the whole arterial network. Note that reflected waves from arterial bifurcations are taken also directly into account (not through $\mathbf{u}_c$), through the eigenfunction expansion (28) of the flow pulse. An incompressible fluid (see Eq. (2)) satisfies the following identity:

$$\nabla\left(\mathbf{u}_c \cdot \mathbf{u}\right) = \mathbf{u}_c \cdot \nabla\mathbf{u} + \mathbf{u}_c \times \boldsymbol{\omega} \tag{64}$$

Then, using Eq. (64), substitution of Eq. (5) and the constitutive law (3) into Eq. (1) results in:

$$\mu_b \nabla^2\mathbf{u} - \mathcal{L}\left(\rho_b \mathbf{u}_{,t} + \rho_b \mathbf{u}_c \cdot \nabla\mathbf{u} - \nabla P_* + \mathbf{f}_h\right) = \mathbf{0}, \tag{65}$$

with

$$P_* = P + \tfrac{1}{2}\rho_b\, u^2 - \rho_b\, \mathbf{u}_c \cdot \mathbf{u}\,, \tag{66}$$

the total pressure, where $(\,)_{,t} \equiv \partial/\partial t$ and similarly for higher derivatives. Eq. (65) is quasi-linear, since the nonlinearities enter in P_* from Eq. (66). In order to facilitate further the analysis and without loosing any of the physical reasoning, we neglect the second order spatiotemporal effects, namely $\mathcal{L}\mathbf{u}_c \cdot \nabla\mathbf{u} \simeq \mathbf{u}_c \cdot \nabla\mathbf{u}$. This differs from the more suitable approximation:

$$\mathcal{L}\left(\rho_b\, \mathbf{u}_{,t} + \rho_b\, \mathbf{u}_c \cdot \nabla\mathbf{u} - \nabla P_* + \mathbf{f}_h\right) \simeq \mathcal{L}\left(\rho_b\, \mathbf{u}_{,t}\right) + \rho_b\, \mathbf{u}_c \cdot \nabla\mathbf{u} - \nabla P_* + \mathbf{f}_h, \tag{67}$$

only with respect to the definition, either of $\mathbf{f}_h$, or the arbitrary function $P_s(t)$ in Eq. (21) that satisfies the constraint (70) below. Then, due to (67), Eq. (65) reads:

$$\mu_b\, \nabla^2\mathbf{u} - \rho_b\, t_b \mathbf{u}_{,tt} - \rho_b\, \mathbf{u}_{,t} - \rho_b\, \mathbf{u}_c \cdot \nabla\mathbf{u} - \nabla P_* + \mathbf{f}_h = \mathbf{0}\,. \tag{68}$$

Lopez et al. [26] used Eq. (68) in linear studies of Maxwell fluids, and Quintanilla and Rajagopal [40] in similar studies of Burgers fluids, when the convective acceleration vanishes ($P_* = P$, $\mathbf{u}_c = \mathbf{0}$). Taking the curl of Eq. (68) yields the vorticity equation:

$$\mu_b\, \nabla^2\mathbf{A} - \rho_b\, t_b\, \mathbf{A}_{,tt} - \rho_b\, \mathbf{A}_{,t} - \rho_b\, \mathbf{u}_c \cdot \nabla\mathbf{A} + \mathbf{A}_h = \mathbf{K}\,, \tag{69}$$

with $\mathbf{K}$ an arbitrary harmonic vector potential $\left(\nabla^2\mathbf{K} = \mathbf{0}\right)$. This rather simple form of the vorticity equation emerges, since we selected the vector potentials $\mathbf{A}$ and $\mathbf{A}_h$ to belong to the same gauge: $\nabla \cdot \mathbf{A} = 0$, $\nabla \cdot \mathbf{A}_h = 0$. We avoid harmonic effects, in our an-harmonic analysis, by setting $\mathbf{K} = \mathbf{0}$ in Eq. (69), which results in Eq. (20). Thereupon, taking the curl of Eq. (20) and subtracting from Eq. (68) yields:

$$\nabla P_* = 0. \tag{70}$$

Eq. (70) reduces, using Eq. (66), to the generalized Bernoulli's Eq. (21).

Appendix B. **The radial displacement decomposition.** Since the radial force, F_b, that blood exerts on the endothelium, includes the solitary time pulse, $p_s(\tau_a)$, we can decompose the radial displacement, $\bar{\xi}$, as:

$$\bar{\xi}(\tau_a,\, \eta_a) \;=\; \bar{\xi}_s(\tau_a) + G(\tau_a,\, \eta_a), \tag{71}$$

$$G(\tau_a,\, \eta_a) \;=\; \Psi^{(a)}(\tau_a,\, \eta_a) + \Theta(\tau_a,\, \eta_a). \tag{72}$$

$G(\tau_a,\, \eta_a)$ is the Green's function for of the inhomogeneous problem (41). The last two Eqs. (19) apply to each term in Eqs. (71-72), which in dimensionless form read:

$$\bar{\xi}_i(\tau_a = 0, \eta_a) = 0, \quad \frac{\partial\bar{\xi}_i(\tau_a = 0, \eta_a)}{\partial\tau_a} = 0,\; i = \{1, 2, 3\}, \tag{73}$$

where $\bar{\xi}_1 \equiv \bar{\xi}_s$, $\bar{\xi}_2 \equiv \bar{\Psi}$, $\bar{\xi}_3 \equiv \Theta$. Hence, due to the dimensionless parameters of Eqs. (42) and with substitution of Eq. (71) into (41) we obtain the decomposed problem:

$$\frac{d^2\bar{\xi}_s(\tau_a)}{d\tau_a^2} + \frac{1}{\varepsilon_a\, De_a}\frac{d\bar{\xi}_s(\tau_a)}{d\tau_a} = p_s(\tau_a) - p_{\mathrm{ref}}, \tag{74}$$

$$\frac{\partial^2\Psi^{(a)}}{\partial\tau_a^2} - \frac{\partial^2\Psi^{(a)}}{\partial\eta_a^2} + \frac{1}{\varepsilon_a\, De_a}\frac{\partial\Psi^{(a)}}{\partial\tau_a} + \frac{\bar{h}}{\varepsilon_a}\Psi^{(a)} = 0, \tag{75}$$

$$\frac{\partial^2\Theta}{\partial\tau_a^2} - \frac{\partial^2\Theta}{\partial\eta_a^2} + \frac{1}{\varepsilon_a\, De_a}\frac{\partial\Theta}{\partial\tau_a} + \frac{\bar{h}}{\varepsilon_a}\Theta = \frac{F_d}{\varepsilon_a^2}. \tag{76}$$

Eq. (74) has the solution (46). Note that Eq. (46) satisfies the initial conditions (73) for $i = 1$. Eq. (75), with the aid of the transformation:

$$\Psi^{(a)} = \mathrm{e}^{-\tau_a/(2\varepsilon_a)}\, \Phi^{(a)}(\tau_a,\, \eta_a), \tag{77}$$

and after lengthy, but straightforward calculations [44], admits a similar an-harmonic solution to the flow problem in the form of (47)-(50). According to standard Green's function techniques [37], the solution of the Cauchy problem for Eq. (76), in $-\infty < \eta_a < \infty$, with homogeneous, initial conditions (73) for $i = 3$, is of the form (51-53).

Received November 18, 2010; Accepted April 11, 2011.

E-mail address: pvolter@cs.uoi.gr
E-mail address: acharala@cc.uoi.gr
E-mail address: fotiadis@cs.uoi.gr
E-mail address: lmihalis@cc.uoi.gr